

Macroscopic Modelling and Simulation of ACC and CACC Traffic

Ioannis K. Nikolos
School of Production
Engineering & Management
Technical University of Crete
Chania, Crete, Greece 73100
Email: adelis@science.tuc.gr

Anargiros I. Delis
School of Production
Engineering & Management
Technical University of Crete
Chania, Crete, Greece 73100
Email: jnikolo@dpem.tuc.gr

Markos Papageorgiou
School of Production
Engineering & Management
Technical University of Crete
Chania, Crete, Greece 73100
Email: markos@dssl.tuc.gr

Abstract—The incorporation of a macroscopic approach reflecting Adaptive Cruise Control (ACC) and Cooperative Adaptive Cruise Control (CACC) traffic dynamics in a gas-kinetic (GKT) traffic flow model is presented. The approach is a novel one and is based on the introduction of a relaxation term that satisfies the time/space-gap principle of ACC or CACC systems. The relaxation time is assigned on multiple leading vehicles in the CACC case; whereas in the ACC case this relaxation time is only assigned to the direct leading vehicle. Numerical simulations investigate the effect of ACC and CACC to traffic flow macroscopic stability with respect to perturbations introduced in a ring road and to flow characteristics in open freeways with merging flows at an on-ramp. Following from the results, it can be deduced that CACC vehicles increase the stabilization of traffic flow, compared to ACC ones. Further, the proposed CACC approach can further improve the dynamic equilibrium capacity and traffic dynamics, especially at on-ramp bottlenecks.

I. INTRODUCTION

Vehicle Automation and Communication Systems (VACS), such as Adaptive Cruise Control (ACC) and Cooperative Adaptive Cruise Control (CACC) systems, are likely to revolutionize the way traffic flow will be controlled and optimized in the near future. Although such technologies have been developed to increase driver's comfort and safety, the continuously increasing use of such systems in the years to come will have a direct impact on the overall traffic flow. The main aim of an ACC system is to liberate the driver from the need to adjust its speed to that of the leader by forcing the vehicle to slow down when the leading vehicle has a lower speed and, reversely, allows the vehicle to accelerate to a pre-determined speed when the leading vehicle accelerates. In principle, the pre-specified parameters of an ACC system are the time-gap to the leading vehicle, their speed variance, and the speed of the vehicle. However, the application of ACC systems, and for certain parameter settings, may also induce negative effects on traffic flow dynamics. Hence, and to minimize potential negative effects, it is crucial to evaluate the impact of such systems on traffic flow dynamics in advance. Vehicles equipped with CACC systems have the ability of sharing traffic information via vehicular networks or wireless technologies that allow communication between such vehicles. Compared to ACC, the literature on CACC systems is still very premature and relevant studies, usually, do not explore the effects of CACC in traffic flow quantitatively in terms of throughput, capacity, and

congestion reduction but aim on creating design frameworks, to optimize and standardize the use of such technology.

Although much work has been reported for the microscopic simulation of ACC/CACC systems at vehicle level, model applications of macroscopic traffic flow models for the simulation of VACS are relatively rare. Very recently, and closely related to the present work, in [6], [5] macroscopic models proposed to describe the operations of ACC and CACC in the traffic flow. Using linear and nonlinear stability analysis it was found that CACC vehicles enhance the stabilization of traffic flow with respect to both small and large perturbations, compared to ACC vehicles, while numerical simulation supported the analytical findings. The present work aims to contribute to the macroscopic modeling of traffic flow consisting of ACC or CACC vehicles, along with appropriate numerical approximations; it builds on a previous work of the authors in [1] where a unified methodology was proposed for the numerical simulation of several, widely applied, second-order non-equilibrium macroscopic models. Here, the GKT second-order traffic flow model, [8], [2], [9], is utilized as a basis to import and access the macroscopic simulation of ACC/CACC traffic. ACC and CACC effects are incorporated as source terms to the second ("momentum") equation of the system of partial differential equations forming the GKT model, which controls the speed dynamics. One major difference between our approach and that from [6] is that the ACC/CACC term in [6] contributes to the so-called convection term in the momentum equation whereas in our approach the corresponding term contributes to the relaxation term in the GKT model equations. Moreover, in our modeling approach the time-gap parameter, which is an important characteristic of such systems, is explicitly taken into account. The main contributions of the present work can be summarized as: (a) to derive a novel macroscopic approach to model ACC and CACC equipped vehicles with the GKT model and (b) to qualitatively assess its performance through numerical simulations for various traffic flow scenarios for manually driven and ACC/CACC equipped vehicles.

II. THE GKT MODEL AND ADAPTIVE CRUISE CONTROL

The macroscopic model extended here is the gas-kinetic-based traffic flow model (GKT model), from [8], [2], [9]. This model has been shown to describe realistic characteristic properties of traffic flows. By denoting $\rho(x, t)$ the traffic density, $u(x, t)$ the average speed and $q = \rho u$ the traffic flow

rate as functions in space, x , and time, t , the GKT model in conservation law form with source terms is given as,

$$\partial_t \rho + \partial_x (\rho u) = r_{rmp}, \quad (1)$$

$$\partial_t (\rho u) + \partial_x (\rho u^2 + \theta \rho) = \rho \left(\frac{V_e^*(\rho) - u}{\tau} \right) [1 - \beta F(\rho)] + h_{rmp} + \alpha \mathcal{V}_{acc}. \quad (2)$$

In (2) we have also introduced the modeling of ACC and CACC cars via terms $\alpha \mathcal{V}_{acc}$ and $[1 - \beta F(\rho)]$, which will be explained later. Setting $\alpha = \beta = 0$ in these terms, the GKT model equations for manually driven cars are obtained and will be explained first.

In equation (2), $\theta = A(\rho)u^2$ is a pressure-like term, with $A(\rho)$ being a density-dependent variance factor given by the Fermi function as:

$$A(\rho) = A_0 + \delta A \left[1 + \tanh \left(\frac{\rho - \rho_{cr}}{\delta \rho} \right) \right] \quad (3)$$

in which, ρ_{cr} is the critical density, that reflects the boundary between free flow and congested traffic, with A_0 and $A_0 + 2\delta A$ the variance pre-factors between the two states; while $\delta \rho$ denotes the width of the transition region. Typical range of values for the constants A_0 , δA and $\delta \rho$, along with typical range of the other parameters for this model can be found, for example, in [8], [2], [5], [6], [9], [1]. The model includes a traffic relaxation term aiming to keep flow in equilibrium, with $V_e^* \equiv V_e^*(\rho, u, \rho_a, u_a)$ being the, non-local and dynamic, equilibrium speed and τ being a relaxation time. V_e^* depends also on the non-local density ρ_a and mean speed u_a , and is defined as

$$V_e^* = u_{\max} \left[1 - \frac{\theta + \theta_a}{2A(\rho_{\max})} \left(\frac{\rho_a T}{1 - \rho_a / \rho_{\max}} \right)^2 B(\delta u) \right]. \quad (4)$$

According to (4), V_e^* is given by the maximum velocity u_{\max} , reduced by a term that reflects necessary deceleration maneuvers. Both ρ_a and u_a are computed at an anticipated location $x_a = x + \gamma(1/\rho_{\max} + T \cdot u)$ with T being the desired time-gap and γ a scale factor. Further, $B(\delta u)$ is a so-called Boltzmann interaction factor, which, with $\delta u = \frac{u - u_a}{\sqrt{\theta + \theta_a}}$, is defined as

$$B(\delta u) = 2 \left[\delta u \frac{e^{-\delta u^2/2}}{\sqrt{2\pi}} + (1 + \delta u^2) \int_{-\infty}^{\delta u} \frac{e^{-y^2/2}}{\sqrt{2\pi}} dy \right].$$

This term describes the dependence of the braking interaction on the dimensionless velocity difference δu between the actual location x and the anticipation location x_a .

Finally, and following [9], the source term r_{rmp} in the continuity equation (1) denotes the effective source density from on-ramps (or off-ramps) with merging (diverging) length l_{rmp} and inflow $q_{rmp} > 0$ from (or outflow $q_{rmp} < 0$ to) the ramp, and is given as $r_{rmp}(x, t) = q_{rmp}(t)/l_{rmp}$ for x within merging (diverging) zones and zero elsewhere. Further, in equation (2), h_{rmp} describes changes of the macroscopic local speed by assuming that on-ramp vehicles merge to the main road at speed $u_{rmp} < u$ and, conversely, that drivers reduce their speed to u_{rmp} before leaving the main road. Hence, this term is given as

$$h_{rmp}(x, t) = \frac{q \cdot r_{rmp}}{\rho} + \frac{(u_{rmp} - u)|q_{rmp}|}{l_{rmp}}. \quad (5)$$

The main difference between the GKT model and other macroscopic traffic flow models is its non-local character. The non-local relaxation term from (4) is forwardly directed and, therefore, more realistic. In contrast to other macroscopic models, the steady-state speed-density relation, $V^e(\rho)$, is not explicitly given, but results from the steady-state on homogeneous roads.

Next a novel approach to modeling ACC and CACC effects in the model equations is presented. This is done through the terms $\alpha \mathcal{V}_{acc}$ and $[1 - \beta F(\rho)]$ in equation (2), with $\alpha = 1$ and $\beta = 1$. One major difference between this new approach compared to others, e.g. from [6], is that in our approach the corresponding term contributes to the non-local relaxation term in the model equations. Moreover, in our approach the time-gap parameter, which is an important characteristic of such systems, is explicitly taken into account. The ability to explicitly define the time-gap in our approach enables the model to simulate ACC/CACC flows with different time-gap settings, which lead to different dynamic behavior and equilibrium capacities.

We derive our approach on the basis of the control objectives that an ACC system should follow, in accordance to [7]:

- I. To travel with the maximum speed, set by the driver, in cases where no leading vehicles exist in the range covered by the sensors, or leading vehicles exist within range but their velocities are higher than the maximum speed set by the user (*speed control mode*).
- II. To maintain vehicle speed equal to the speed of the leading vehicle at a specified distance, when the leading vehicle is in range and its speed is lower than the maximum speed set by the driver (*gap control mode*).
- III. Transitions between the two aforementioned objectives should be as smooth as possible, in order not to cause discomfort to the passengers, due to abrupt accelerations or decelerations.

Before we proceed, and to avoid confusion, we need to clarify the terms *headway* and *time-gap*. *Time/space-headway* is the time/space distance between the front bumper of the preceding vehicle and the front bumper of the following vehicle, while *time/space-gap* is the time/space distance between the rear bumper of the preceding vehicle and the front bumper of the following one. In a Constant Time Headway (CTH) policy the inter-vehicle spacing is a linear function of the vehicle's speed, which feels more natural to the passengers of the ACC equipped vehicle.

To satisfy the above objectives, the proposed model is based on the following assumptions:

- (1) For densities clearly below a threshold ρ_{acc} (being lower than or equal to ρ_{cr}) the additional terms in the model have no effect, as it is supposed that (on average) the drivers set their maximum speeds (or react) as in a manual manner, i.e. as the GKT model describes (emulating in that way the speed control mode). In the region around ρ_{acc} , a smooth but fast transition between the previous case and the ACC/CACC-controlled situation takes place, described using again the

Fermi function $F(\rho) = 0.5 [1 + \tanh(\rho - \rho_{acc}/\Delta\rho)]$ and to achieve this fast transition, the transition width $\Delta\rho$ takes values of $\Delta\rho \approx 0.025\rho_{max}$, leading to a steep transition between the two states.

(2) During the gap control mode, a constant time gap T^* is desired, which is imposed through its corresponding effect on a desired density ρ^* as

$$\rho^* = \frac{1}{1/\rho_{max} + T^* u^*}, \quad (6)$$

where the denominator is the desired space headway, with $1/\rho_{max}$ reflecting the vehicle length and $u^* = u(x^*)$ is the speed of the preceding vehicle, computed at position

$$x^* = x + \gamma^*(1/\rho_{max} + T^* \cdot u), \quad \gamma^* \in [1, 2].$$

The desired speed relaxes to the speed of the preceding vehicle u^* after a relaxation time τ^* . As a result, the corresponding source term can be modeled for ACC vehicles as:

$$\mathcal{V}_{acc}(\rho, u, \rho^*, u^*) = F(\rho) \left(\frac{\rho^* u^* - \rho u}{\tau^*} \right) \quad (7)$$

In [4] it was demonstrated that the minimum time-gap that can be achieved by ACC vehicles is $0.8s$. In general, indicative values used for ACC traffic are $T^* \in [0.8, 2.2]s$, following [ISO 15622,2010] standards, and $\tau^* \approx 1s$.

For CACC vehicles a similar approach is used, but the corresponding source term takes into account the speeds of more than one preceding vehicles, with a different time relaxation for each one of them. The ability for the system to look downstream increases the smoothing effect of the corresponding source term. Furthermore, this additional information from far downstream allows for the use of lower values of time gaps (without compromising safety), which was also used in the present study. For example, in [10], it was identified that CACC vehicles enable closer vehicle following, with time-gap as low as $0.5 s$. As reduced time gaps are only achievable between vehicles that are equipped with the CACC technology the market penetration rate for these systems plays an important role. Thus, we propose for CACC traffic

$$\mathcal{V}_{cacc}(\rho, u, \rho^*, u^*) = F(\rho) \sum_{i=1}^M \left(\frac{\rho^* u_i^* - \rho u}{\tau_i^*} \right) \quad (8)$$

where $u_i^* = u(x_i^*)$ with $x_i^* = x + i \cdot \gamma^*(1/\rho_{max} + T^* \cdot u)$, $i = 1, \dots, M$, and

$$\rho^* = \frac{1}{1/\rho_{max} + T^* u_1^*}.$$

The parameter values used in this work for CACC traffic are $M = 3$ with $[\tau_1^*, \tau_2^*, \tau_3^*] = [2, 3, 6]$.

III. THE RELAXATION APPROACH AND ITS NUMERICAL DISCRETIZATION

Model equations (1)-(2) can be written in vector form, supplied with initial conditions, as

$$\begin{aligned} \partial_t \mathbf{u} + \partial_x \mathbf{f}(\mathbf{u}) &= \mathbf{s}(\mathbf{u}), \\ \mathbf{u}(x, 0) &= \mathbf{u}_0(x), \end{aligned} \quad (9)$$

where the functions \mathbf{u} , $\mathbf{f}(\mathbf{u})$ and $\mathbf{s}(\mathbf{u}) \in \mathbb{R}^2$ with $\mathbf{u} = [\rho, q]^T$, $\mathbf{f}(\mathbf{u}) = [\rho u, \rho u^2 + \theta \rho]^T$ and $\mathbf{s}(\mathbf{u}) = [r_{rmp}, [1 - \beta F(\rho)](\rho V_e^* - \rho u)/\tau + h_{rmp} + \alpha \mathcal{V}_{acc}]^T$.

Systems in the form of (9) can be rewritten in quasi-linear form

$$\partial_t \mathbf{u} + \mathbf{J}(\mathbf{u}) \partial_x \mathbf{u} = \mathbf{s}(\mathbf{u}), \quad (10)$$

where $\mathbf{J}(\mathbf{u}) = \frac{\partial \mathbf{f}}{\partial \mathbf{u}}$ is the Jacobian matrix of the system. This Jacobian matrix has two distinct, real and positive eigenvalues, for all physically reasonable parameter sets, given as

$$\lambda_{1,2} = u + \frac{1}{2} \frac{\partial P}{\partial q} \pm \sqrt{\left(\frac{1}{2} \frac{\partial P}{\partial q} \right)^2 + \frac{q}{r} \frac{\partial P}{\partial q} + \frac{\partial P}{\partial \rho}}, \quad (11)$$

which denote that the model equations constitute a strictly hyperbolic set of partial differential equations.

Here we briefly present the class of relaxation models of [3] applied to various second-order macroscopic traffic flow models in [1]. Introducing the artificial variables \mathbf{w} , the, corresponding to (9), relaxation system reads as

$$\begin{aligned} \partial_t \mathbf{u} + \partial_x \mathbf{w} &= \mathbf{s}(\mathbf{u}), \\ \partial_t \mathbf{w} + \mathbf{C}^2 \partial_x \mathbf{u} &= \frac{\mathbf{f}(\mathbf{u}) - \mathbf{w}}{\epsilon}, \end{aligned} \quad (12)$$

and the extra initial condition $\mathbf{w}(x, 0) = \mathbf{w}_0(x) = \mathbf{f}(\mathbf{u}_0(x))$, where the small parameter ϵ ($0 < \epsilon \ll 1$), is the *relaxation rate* and $\mathbf{C}^2 = \text{diag}\{c_1^2, c_2^2\}$ is a positive diagonal matrix. Applying the Chapman-Enskog expansion in system (12), the following approximation for \mathbf{u} can be obtained,

$$\begin{aligned} \partial_t \mathbf{u} + \partial_x \mathbf{f}(\mathbf{u}) &= \mathbf{s}(\mathbf{u}) + \epsilon \partial_x \left[\left(\frac{\partial \mathbf{f}(\mathbf{u})}{\partial \mathbf{u}} \right) \mathbf{s}(\mathbf{u}) \right] + \\ &+ \epsilon \partial_x \left[\left(\mathbf{C}^2 - \left(\frac{\partial \mathbf{f}(\mathbf{u})}{\partial \mathbf{u}} \right)^2 \right) \partial_x \mathbf{u} \right] + O(\epsilon^2). \end{aligned} \quad (13)$$

Equation (13) controls the first-order behavior of system (12), with the third term on the right-hand side being an $O(\epsilon)$ dominant dissipation term in the model with $\left(\mathbf{C}^2 - \left(\frac{\partial \mathbf{f}(\mathbf{u})}{\partial \mathbf{u}} \right)^2 \right)$ being the diffusion-like coefficient matrix. Model (12) is well-posed only if this matrix is positive semi-definite for all \mathbf{u} . This requirement on the diffusion coefficient matrix is the well-known *sub-characteristic condition* [3], i.e.

$$\mathbf{C}^2 - \left(\frac{\partial \mathbf{f}(\mathbf{u})}{\partial \mathbf{u}} \right)^2 \geq 0, \quad \forall \mathbf{u}. \quad (14)$$

Condition (14) can always be satisfied by choosing sufficiently large values for the elements in \mathbf{C}^2 , for \mathbf{u} varying in a bounded domain. As such, the solution of the relaxation model (12) converges strongly to the unique entropy solution of the original conservation laws. In practice this can be equivalent to the choice

$$\lambda^2 \leq c^2, \quad \text{where } \lambda = \max_{1 \leq i \leq 2} |\lambda_i| \text{ and } c = \min_{1 \leq i \leq 2} |c_i|. \quad (15)$$

Now, system (12) can be easily diagonalized leading to the following decoupled system of equations:

$$\begin{aligned} \partial_t (\mathbf{w} + \mathbf{C} \mathbf{u}) + \mathbf{C} \partial_x (\mathbf{w} + \mathbf{C} \mathbf{u}) &= \frac{\mathbf{f}(\mathbf{u}) - \mathbf{w}}{\epsilon} + \mathbf{C} \mathbf{s}(\mathbf{u}); \quad (16) \\ \partial_t (\mathbf{w} - \mathbf{C} \mathbf{u}) - \mathbf{C} \partial_x (\mathbf{w} - \mathbf{C} \mathbf{u}) &= \frac{\mathbf{f}(\mathbf{u}) - \mathbf{w}}{\epsilon} - \mathbf{C} \mathbf{s}(\mathbf{u}). \quad (17) \end{aligned}$$

The left-hand side of system (16)-(17) is linear with constant wave speeds. Its solution has the property that it propagates at finite speeds along linear characteristic curves $dx/dt = \pm C$. From (16)-(17) and by setting $\mathbf{g}_{1,2} = \mathbf{w} \pm C\mathbf{u}$, the follow relations to the original variables of the relaxation system hold,

$$\mathbf{u} = \frac{1}{2}C^{-1}(\mathbf{g}_1 - \mathbf{g}_2) \quad \text{and} \quad \mathbf{w} = \frac{1}{2}(\mathbf{g}_1 + \mathbf{g}_2). \quad (18)$$

The structure of the linear characteristic field of the relaxation system constitutes a clear advantage compared to the original conservation laws for their numerical integration.

For the spatial discretization of (12) the finite volume approach is adopted. Let $x_i = i\Delta x$, $x_{i\pm\frac{1}{2}} = (i \pm \frac{1}{2})\Delta x$, where Δx is a uniform spatial discretization step. The discrete cell average of \mathbf{u} in the cell $I_i = [x_{i-\frac{1}{2}}, x_{i+\frac{1}{2}}]$ at time t is defined as $\mathbf{u}_i(t)$ and the approximate value of \mathbf{u} at $(x_{i+\frac{1}{2}}, t)$ by $\mathbf{u}_{i+\frac{1}{2}}(t)$. The semi-discrete relaxation system is given as

$$\begin{aligned} \frac{\partial}{\partial t}\mathbf{u}_i + \frac{1}{\Delta x}(\mathbf{w}_{i+\frac{1}{2}} - \mathbf{w}_{i-\frac{1}{2}}) &= \mathbf{r}(\mathbf{u})_i, \\ \frac{\partial}{\partial t}\mathbf{w}_i + \frac{C^2}{\Delta x}(\mathbf{u}_{i+\frac{1}{2}} - \mathbf{u}_{i-\frac{1}{2}}) &= -\frac{1}{\epsilon}(\mathbf{w}_i - \mathbf{f}(\mathbf{u})_i). \end{aligned} \quad (19)$$

where $\mathbf{r}(\mathbf{u})_i$ and $\mathbf{f}(\mathbf{u})_i$ are discrete averages of the source term and flux function, respectively. To completely define the spatial discretization, we need to compute the flux values $\mathbf{u}_{i\pm\frac{1}{2}}$ and $\mathbf{w}_{i\pm\frac{1}{2}}$. As system (12) has linear characteristics and its characteristic speeds, $+c_k$ and $-c_k$, are constant, the construction of an upwind scheme is much simpler than developing such a scheme for the original nonlinear conservation laws. For example, the *first-order upwind* scheme, [3], [1], applied to \mathbf{g}_1 and \mathbf{g}_2 gives $\mathbf{g}_{1,i+\frac{1}{2}} = \mathbf{g}_{1,i}$ and $\mathbf{g}_{2,i+\frac{1}{2}} = \mathbf{g}_{2,i+1}$.

For increasing the spatial order of accuracy, a WENO-type interpolant approach is applied, where the approximate solution is reconstructed using higher-order polynomials. By direct application of this reconstruction to the k -th components of the characteristic variables, $\mathbf{g}_{1,2} = \mathbf{w} \pm C\mathbf{u}$, a non-oscillatory higher-order spatial discretization is obtained. The superiority of applying higher-order schemes, compared to low-order ones, in traffic flow simulations has been recently demonstrated in [1]. By applying a fifth-order WENO reconstruction the discrete values of each component of $\mathbf{g}_{1,i+\frac{1}{2}}$ and $\mathbf{g}_{2,i+\frac{1}{2}}$, at a cell boundary $i+\frac{1}{2}$, are defined as left and right extrapolated values $\mathbf{g}_{1,i+\frac{1}{2}}^-$ and $\mathbf{g}_{2,i+\frac{1}{2}}^+$ i.e., $\mathbf{g}_{1,i+\frac{1}{2}} = \mathbf{g}_{1,i+\frac{1}{2}}^-$ and $\mathbf{g}_{2,i+\frac{1}{2}} = \mathbf{g}_{2,i+\frac{1}{2}}^+$. After the reconstructions have been performed to each component of the characteristic variables, the numerical fluxes for $\mathbf{u}_{i+\frac{1}{2}}$ and $\mathbf{w}_{i+\frac{1}{2}}$ are computed from (18). In a similar manner we compute the face values at cell boundary $i - \frac{1}{2}$.

The semi-discrete relaxation system (19) constitutes a system of autonomous ordinary differential equations with a stiff relaxation term. A time marching approach based on implicit-explicit (IMEX) Runge-Kutta (RK) splitting was considered as to avoid the time step restrictions imposed by an explicit solver due to stiffness. As such, the explicit RK scheme treats the non-stiff stage of the splitting while a diagonally implicit RK scheme treats the stiff one. We note that even though an implicit scheme is used, either linear or nonlinear algebraic equations have to be solved due to the special structure of the

relaxation system. The choice of the time marching step Δt^n is based only on a usual CFL condition,

$$CFL = \max\left(\left(\max_{i,k} c_k^n\right) \frac{\Delta t^n}{\Delta x}, \frac{\Delta t^n}{\Delta x}\right) \leq \frac{1}{2},$$

where the values of the relaxation constants c_k^n are re-computed at each time step based on the Jacobian eigenvalues as to satisfy the sub-characteristic condition (14). For a detailed presentation of the spatial and temporal discretizations, as well as the treatment of boundary conditions and source term computations, we refer to [1].

IV. NUMERICAL SIMULATIONS AND DISCUSSION

We investigate numerically the performance of the models presented, which aim to describe the traffic flow dynamics for the different vehicle types such as, manually driven, ACC and CACC vehicles. We consider two test cases. The first one is for traffic flows on a circular homogeneous freeway where we aim to examine the formation of traffic instabilities with respect to perturbations introduced in the flow field. The second category of test cases is the simulation of a freeway with an on-ramp i.e. a potential bottleneck. For all numerical tests presented next, the relaxation rate $\epsilon = 10^{-8}$ and the CFL value to 0.4.

A. Homogeneous Traffic with a Localized Perturbation

For this test case we assume that the traffic flow is in a ring of circumference of $L = 10km$. Following [8], [2], [6], [1], we consider a dipole-like initial variation of the average density $\bar{\rho}$ given as

$$\rho(x, 0) = \bar{\rho} + \Delta\rho \left[\cosh^{-2}(D) - \frac{x^+}{x^-} \cosh^{-2}(E) \right] \quad (20)$$

where $D = (x - x_0)/x^+$ and $E = (x - x_0 - \Delta x_0)/x^-$ with $x^+ = 201.5$ and $x^- = 805m$ and $\Delta x_0 = x^+ + x^-$. The initial flow $q(x, 0) = q_e(\rho(x, 0)) = \rho V^e(\rho)$ is assumed in local equilibrium. The induced perturbation eventually leads to instabilities for given values of $\bar{\rho}$. This can be understood also intuitively, at larger densities a higher percentage of drivers that approach a density peak must brake, thus increasing the density peak. The ring was discretized with $npts = 400$ grid points. The model parameters used in the simulations were $u_{max} = 110$ km/h, $\rho_{max} = 160$ veh/km, $\rho_{cr} = 0.27\rho_{max}$, $\tau = 35s$, $A_0 = 0.008$, $\delta A = 0.02$, $\delta\rho = 0.1\rho_{max}$, $T = 1.8s$ and $\gamma = 1.2$. Simulations are reported up to final time of 1200s. The scenario presented here is for $\bar{\rho} = 35$ and $\Delta\rho = 6$ veh/km. A cascade of traffic jams emerges, i.e. stop-and-go traffic, as can be seen in Fig. 1 for manually driven cars.

In Fig. 2 the spatio-temporal evolution using the proposed ACC and CACC approaches are shown. The coefficient used are $\tau^* = 1$ for ACC and $[\tau_1^*, \tau_2^*, \tau_3^*] = [2, 3, 6]$ for CACC traffic. The value for $\rho_{acc} = 0.9\rho_{cr}$ and $T^* = 1$ for CACC traffic while for ACC $T^* = 1.2$. We note here that these values for T^* correspond to a more conservative driving behavior, compared to lower values that correspond to more aggressive driving behavior. The ACC traffic is still in the unstable regime, but remains uncongested; while for CACC traffic the initial perturbation rapidly fades out with time, leading to a homogeneous traffic. A similar test and corresponding results can also be found in [6], although for a different modeling and

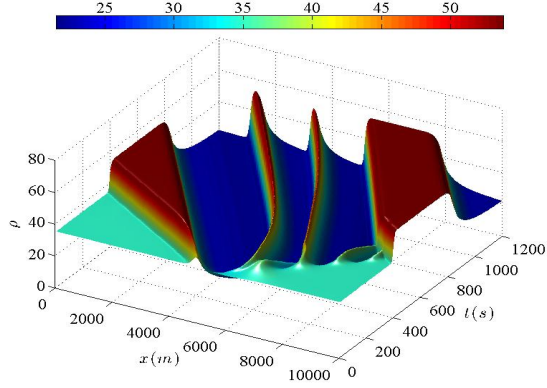


Fig. 1. Density evolution for manual cars for $\bar{\rho} = 35$ and $\Delta\rho = 6$

numerical approach. Referring to Fig. 3, it is important to note the increased traffic flow rate along the total length of the ring road for ACC and CACC traffic, which is more pronounced for CACC traffic, as a result of the imposed desired time gap.

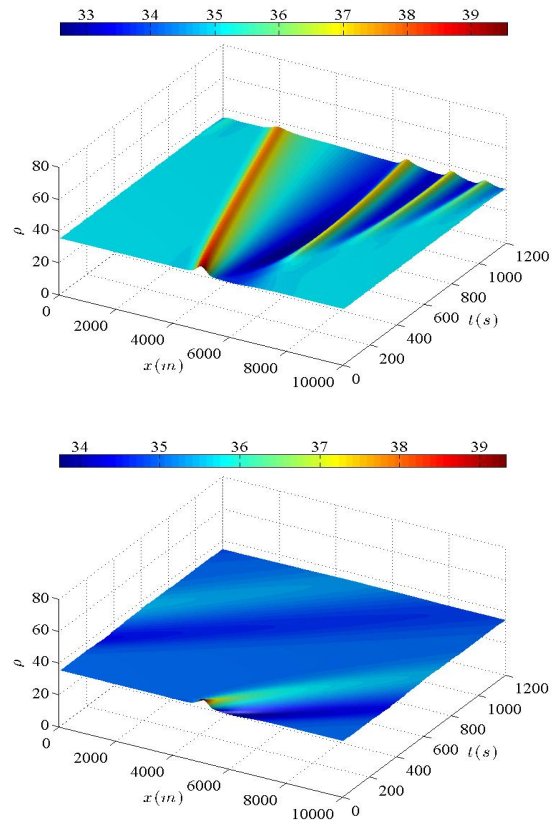


Fig. 2. Density evolution for $\bar{\rho} = 35$ and $\Delta\rho = 6$ for ACC (top) and CACC flows using (7) and (8)

B. Traffic states close to an on-ramp

Different traffic states (i.e. congestion patterns) can be developed close to bottlenecks caused by on-ramps, lane closures, etc. in a freeway, see for example [2], [9]. We simulate a freeway of length $L = 30\text{km}$ with open boundaries

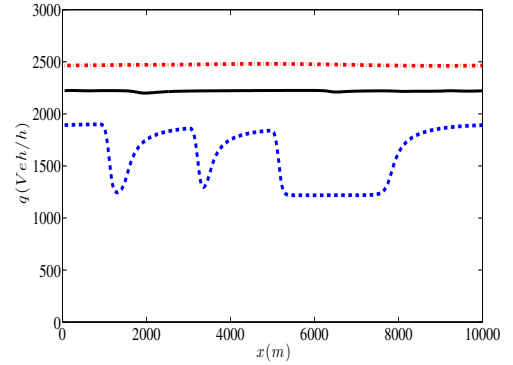


Fig. 3. Flow profiles at $t = 1200$ s for $\bar{\rho} = 35$ and $\Delta\rho = 6$: for ACC (solid black line), CACC (dashed red line) and manual cars

for a total of 150 minutes. Imposing an initial homogeneous equilibrium traffic flow $q_f = 1824.5$ veh/h (which results to $\rho(x, 0) = 30$ veh/km) simulations are performed for an on-ramp inflow $q_{rmp} = 200$ veh/h of length $l_{rmp} = 400\text{m}$ located at $x_{rmp} = 8000\text{m}$ with a merging zone for $x \in [x_{rmp} - l_{rmp}/2, x_{rmp} + l_{rmp}/2]$. The model parameters used in the simulations are, $u_{max} = 110$ km/h, $\rho_{max} = 140$ veh/km, $\rho_{cr} = 0.27\rho_{max}$, $\tau = 40\text{s}$, $A_0 = 0.008$, $\delta A = 0.02$, $\delta\rho = 0.1\rho_{max}$, $T = 1.7\text{s}$ and $\gamma = 1.2$.

The traffic density evolution for manual traffic is presented in Fig. 4. One can observe an Oscillating Congested Traffic (OCT), [2], flow upstream of the ramp and stop-and-go waves downstream. These stop-and-go waves initially travel downstream but at later times start traveling upstream converging to the oscillatory congested region upstream of the ramp. Whenever an upstream traveling jam passes the bottleneck, it triggers a new perturbation

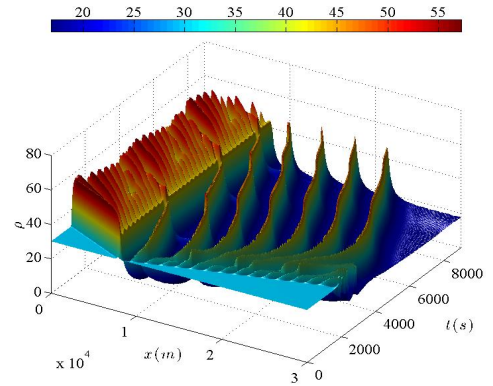


Fig. 4. Density evolution close to an on-ramp for manual cars for $q_{rmp} = 200$ veh/h

In Fig. 5 the spatio-temporal evolution for ACC and CACC traffic is presented and in Fig. 6 the flow rate profiles at $t = 150$ min are compared between each other and those resulted from manual traffic. The ACC traffic becomes non-oscillatory both upstream and downstream of the ramp but a Synchronized Homogeneous Congested Traffic (HCT), [2], region slowly develops upstream, with the downstream flow rate greatly increased. For the CACC traffic the upstream

congestion has completely disappeared and a more pronounced increase in the flow rate is established.

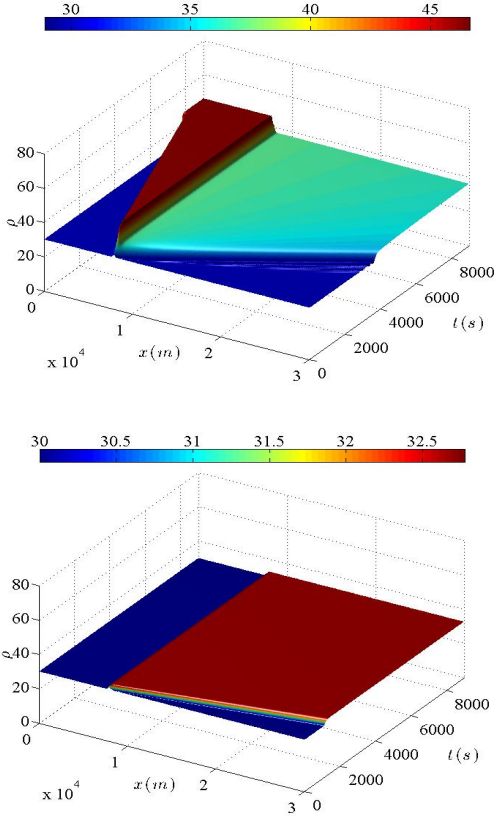


Fig. 5. Density evolution with $q_{rmp} = 200$ veh/h for ACC (top) and CACC traffic

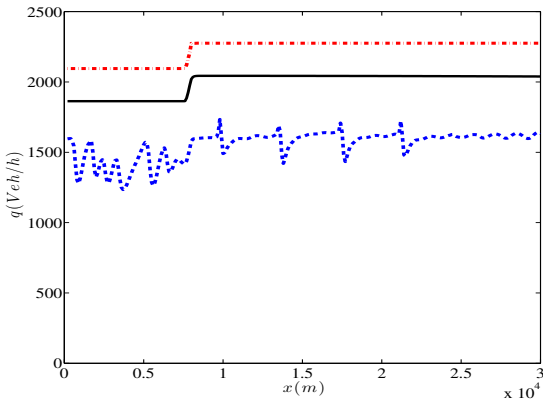


Fig. 6. Flow rate profiles at $t = 150$ min for $q_{rmp} = 200$ veh/h: for ACC (solid black line), CACC (dashed red line) and manual cars

V. CONCLUSIONS

A macroscopic approach to model the dynamics of ACC and CACC traffic flows was presented. To model the impact of ACC and CACC vehicles on traffic flow dynamics the second-order GKT model was used as the basis model since it allows to describe the fluctuations of speed dynamics around a so-called equilibrium speed-density relationship. An important

part of the simulation process is the numerical solution of the resulting models by the application of a high-resolution finite volume relaxation scheme. The approach presented here is based on the introduction of a relaxation term in the momentum equation that satisfies the time/space-gap principle of ACC systems. The relaxation time is distributed over multiple vehicles in the CACC systems whereas in the ACC ones the relaxation time is only related to the direct leading vehicle. Thus, the effects of ACC vehicles have been extended to account for the information exchange between multiple vehicles. We have shown numerically that CACC vehicles enhance the stabilization of traffic flow with respect to introduced perturbations compared to ACC vehicles. The observed enhanced dynamic equilibrium capacity for our CACC system resulted to the suppression of traffic congestion at an on-ramp bottleneck. We postulate that, this approach of jam-avoiding driving by CACC vehicles, which dynamically increases the local capacity near the on-ramp, can be transferred to other kinds of bottlenecks as well thus enhancing traffic operations. Our ongoing work is the numerical investigation of the characteristics of mixed traffic flow consisting of CACC and manual vehicles to assess the contribution of the penetration rate of CACC vehicles to the stabilization of the traffic dynamics. In addition, further validation of the proposed ACC/CACC approach compared to microscopic simulations is under development.

ACKNOWLEDGMENTS

This research was supported by TRAFFIC MANAGEMENT for the 21st century (TRAMAN21) ERC Advanced Investigator Grand under the European Union's Seventh Framework Program (FP/2007-20013)

REFERENCES

- [1] A.I. Delis, I.K. Nikolos and M. Papageorgiou, High-resolution numerical relaxation approximations to second-order macroscopic traffic flow models, *Transportation Research Part C: Emerging Technologies*, vol 44, pp. 318-349, 2014.
- [2] D. Helbing, A. Hennecke, V. Shvetsov and M. Treiber, MASTER: Macroscopic traffic simulation based on a gas-kinetic, non-local traffic model, *Transportation Research Part B: Methodological*, vol 35, pp. 183-211, 2001.
- [3] S. Jin and Z. Xin, The relaxing schemes of conservation laws in arbitrary space dimensions, *Comm. Pure Appl. Math.*, vol. 48, pp. 235-277, 1995.
- [4] G. Marsden G., M. McDonald and M.Brackstone, Towards an understanding of adaptive cruise control, *Transportation Research Part C: Emerging Technologies*, vol. 9, pp. 3351, 2001.
- [5] D. Ngoduy, Application of gas-kinetic theory to modeling mixed traffic of manual and ACC vehicles, *Transportmetrica*, Vol 8, pp.43-60, 2012.
- [6] D. Ngoduy, Instability of cooperative adaptive cruise control traffic flow: A macroscopic approach, *Commun. Nonlinear Sci Numer. Simulat.*, Vol 18, pp. 2838-2851, 2013.
- [7] S.E. Shladover, D. Su and X.-T. Lu, Impacts of Cooperative Adaptive Cruise Control on Freeway Traffic Flow, *Transp. Res. Rec. J. Transp. Res. Board*, vol. 2324, pp. 6370, 2012.
- [8] M. Treiber, A. Hennecke and D. Helbing, Derivation, properties, and simulation of a gas-kinetic-based, nonlocal traffic model, *Physical Review E - Statistical Physics, Plasmas, Fluids, and Related Interdisciplinary Topics*, vol 59, pp. 239-253, 1999.
- [9] M. Treiber and A. Kesting, *Traffic flow dynamics: Data, models and simulation*, Springer, 2013.
- [10] J. VanderWerf, S.E. Shladover, M.A. Miller and N. Kourjanskaia, Evaluation of Adaptive Cruise Control Systems on Highway Traffic Flow Capacity and Implications for Deployment of Future Automated Systems. *Transportation Research Record*, Vol. 1800, pp. 78-84, 2002.